Synthesis and Characterization of Nickel Nanoparticles of Gloriosa Superba and Its Anti-Angiogenic Activity in Cervical Cancer

Mrudhulla S
Bharathiar University
Anjali K Ravi
Bharathiar University
Saradhadevi Muthukrishnan (saradhadevi@buc.edu.in)
Bharathiar University
Velayuthaprabhu Shanmugam
Bharathiar University
Vijaya Anand Arumugam
Bharathiar University
Arun Muthukrishnan
Bharathiar University

Research Article

Keywords: Cervical cancer, Nickel nanoparticles, Gloriosa superba,Angiogenic activity, TEM, Zeta potential.

Posted Date: March 18th, 2022

DOI: https://doi.org/10.21203/rs.3.rs-1456787/v1

Abstract

Cancer is a leading cause of death worldwide that arises from the transformation of normal cells into tumour cells in a multi-stage process. There is always a stable demand for new therapies to treat cancer. Research communities is showing interest towards nanoparticles along with naturally-derived compounds as they are considered as less toxic compared to chemotherapy and radiation. The present study is to develop a fast, eco-friendly synthesis of *Gloriosa superba* nickel nanoparticles (GSNiNPs) using methanolic extract of *Gloriosa superba* tuber which acts as a reducing agent and has an active principle against cancer activity. Nickel nanoparticles are considered as good adsorbents due to their chemical and magnetic properties. The synthesised GSNiNPs were characterized using UV Visible spectroscopy, which showed a prominent peak at 350 nm verified the formation of NiNps by the reduction of bioactive compounds of *Gloriosa superba* towards metal salts. FTIR confirmed that the GSNiNPs were functionalized with biomolecules. SEM and TEM analysis revealed that GSNiNPs are slightly spherical and agglomerated nanoparticles. The *in-vitro* cytotoxic activity of *Gloriosa superba* nickel nanoparticles in HeLa cancer cell lines was analyzed using MTT assay, wound healing assay, DAPI staining and double staining. *In vitro* anti-angiogenic efficacy of *Gloriosa superba*-nickel nanoparticles was evaluated via the expression pattern of caspase 3 and 9, VEGF A and VEGF B through reverse transcriptase-PCR. The results revealed that *Gloriosa superba* nickel nanoparticles possess apoptotic and anti-angiogenic effects in *HeLa* cell lines by inhibiting VEGF A and B and increasing the levels of caspase 3 and 9. GSNiNPs can act as an effective anti-cancer therapeutic agent for cervical cancer cells. In conclusion, the synthesized GSNiNPs can bring a new approach to improve the bioavailability of drug-responsive for the treatment of cervical cancer.

1. Introduction

Cancer is characterized by uncontrolled growth and proliferation of abnormal cells. It is one of the leading causes of death throughout the world. Cancer starts at one point and spreads to other parts of the body is called metastasis [1]. Gynecologic cancer is a type of cancer that affects particularly the woman's reproductive organs which includes cervical, ovarian, uterine, vaginal and vulvar. Of this cervix cancer is the third most common cancer which affects about 1.04 lakhs women during the year 2020 (ICMR 2020). Human papillomavirus (HPV) is the foremost important factor for the cause of cervical cancer in women [2]. Persistent HPV infections cause cancer cell proliferation mainly at the transformation zones between different kinds of epithelium like the cervix, anus, and oropharynx [3]. Other cofactors for the cause of cervical cancer include low immunity, food patterns, lack of exercise, obesity, smoking and use of several birth control pills [4].

Angiogenesis is one of the important biological processes for primary cancer growth and metastasis. The important biological macromolecule (biomarker) that modulates angiogenesis in cervical cancer was the vascular endothelial growth factor (VEGF) [5]. VEGF family members, VEGF-A is one of the most important angiogenic regulators in tumour angiogenesis [6]. VEGF-B binds with a high affinity towards VEGFR-1, but not to VEGFR-2 or -3. Activation of this receptor induces a poor mitogenic signal for

endothelial cells suggesting that VEGF-B is an inefficient endothelial cell mitogen [7].The VEGF, a major mediator of tumour angiogenesis, promotes mobilization of endothelial progenitor cells, cell proliferation, migration, survival, and vascular permeability in cancer cells. VEGF also acts as a survival factor for endothelial cells and tumour cells to protects them from apoptotic activity (Programmed cell death) [6].

Currently, available standard treatments like chemotherapy and radiotherapy were cytotoxic to both cancerous cells and also to normal cells. It causes a lot of side effects by destroying cells that divide rapidly under normal circumstances, disrupts the alimentary canal, damages a cell within the bone marrow, and hair loss [8]. Over the past 20 years, plants with anti-cancer properties have been considered safe and effective without any toxic side effects. Moreover, it has been proved that several medicinal plants and herbs have the efficacy to prevent or reduce the risk of cancer in humans. India features a wealth of medicinal plants most of which are traditionally used in Ayurveda, Unani systems of medicines, and also by the tribal peoples to heal a number of diseases for several generations. The medicinal value of plants lies in some chemical substances like secondary metabolites (alkaloids, flavonoids, tannins, and phenolic) that produces a specific physiological action against various diseases in the human body [9]. Researchers found that plants are a great source for developing new, effective and safe anticancer drugs compared with synthetic ones.

The present study concentrates on the anticancer properties of *Gloriosa superba*is herbaceous perennials with reflexed petals, ranging in colour from a greenish-yellow, yellow, orange, red and deep pinkish-red. It is also called the state flower of Tamil Nadu. It belongs to the family Colchicaceae with the native of tropical Asia and Africa [10]. *Gloriosa superba* is one of the comparatively less explored traditional medicinal plants that have immense application against a number of diseases. Lower doses of super bine and gloriosine found in *G. superba* tubers are used as a purgative, tonic, and anti-abortive, gonorrhea, leprosy, colic, intestinal worms, for promoting labor pain. Colchicine, a predominant bioactive compound present in *G. superba* is used to treat gout and rheumatism. The anticancer and antioxidant efficacy of *Gloriosa superba* silver nanoparticles against DLA tumour cells has been reported by [9].

In spite of its enormous potential to act as an anticancer agent, still, the plant bioactive compounds lack targeted drug delivery, multidrug resistance in tumour cells, poorly soluble in water, and also easily excreted in urine due to their smaller size. To address these issues, studies have been performed to investigate the effects of nano-combinations and medicinal plants for cancer treatment [11]. The nanoparticles act as an ideal vehicle to enhance the permeation and retention in tumor tissue. They gain special attention due to its greater area and volume ratio and have higher efficacy than macromolecules. These nanoparticles do not enter into healthy tissues because of the tight endothelial junction of capillary blood arteries. But in cancer cells, due to its leaky vasculature and inadequate lymphatic damage, the nanoparticles efficiently extravagate and enter into the tumour interstitium in many solid tumours, is known as the EPR effect. The combination of active constituents of plants along with nano vehicles shows good efficacy in reversing the drug resistance, enhancing the curative effects, and reducing adverse reactions [12].

Among various metal nanoparticles like Ni, Cu and Fe, the nickel nanoparticles possess much better applications as catalysts, metallic conductors and magnetic materials. [13]. Nickel nanoparticles (NiNPs) have been widely used in cancer therapy and clinical diagnoses due to their unique structure and properties. The functionalization of NiNPs could enhance the membrane permeability and induce apoptosis in hepatocellular carcinoma cells [14] and HT 29 human lung epithelial cells [15]. Various approaches have been used to prepare the NiNPs such as hydrothermal, precipitation, sol-gel, thermal decomposition and solvothermal [16]. Most of these are non-eco-friendly, produce toxic wastes, and highly expensive methods. Hence, metal nanoparticles are synthesized through green synthesis approaches using plant extracts, enzymes and microorganisms to overcome these issues. Green synthesis of NiNPs using plant extract is considered as an effective method of production of ecofriendly nanoparticles. They are cost effective, easily available, fast and easy method to scale up for large scale production with well-defined morphology, good polydispersity and stability. The bioactive components present in the plant extracts will served as reducing, capping and stabilizing agents in the synthesis of nanoparticle [17].

Based on the previous studies, there is a lack of reports available on the anticancer efficacy of *G. superba* synthesized nickel nanoparticles against cervical cancer, particularly by downregulating the angiogenic activity of VEGF A and B transcription and by increasing the apoptotic levels of caspase 3 and 9 to induce cell death in HeLa cell lines. Hence the present study was designed to characterize the synthesized Nickel nanoparticles of *Gloriosa superba* tuber by UV visible spectroscopy, SEM, TEM, DLS, zeta potential, FTIR and XRD analysis and its anticancer efficacy was evaluated using MTT, wound healing, DAPI, Double staining and RT-PCR techniques in cervical cancer cells. The findings revealed that the synthesized nickel nanoparticles from *Gloriosa superba* induces anti-cancer activity by inhibiting angiogenic activity in HeLa cell lines.

2. Materials And Methods

2.1 Collection of plant sample and preparation of methanolic extracts of Gloriosa superba tuber

The fresh tuber of *Gloriosa superba* was collected from the farm at Pollachi, Coimbatore district, Tamil Nadu. The collected samples were washed thoroughly in tap water, shade dried and finely powdered.Sixty grams of tuber powder of *Gloriosa superba* was filled in thimble using Whatman No.1 filter paper and extracted with 600 ml of methanol using a soxhlet extractor for 24 hours at 60^{o}C. The methanol extract of *Gloriosa superba*tuber (MEGS)was distilled and evaporated by a rotary evaporator to dryness. The concentrated extract of tuber was then accurately weighed and stored for further use.

2.2 Diphenyl-1-picrylhydrazyl (DPPH) radical scavenging activity:

DPPH radical is a widely used method to evaluate the free radical scavenging ability of natural compounds. This assay is based on the measurement of the scavenging ability of antioxidant substances toward the stable radical. Various concentrations of MEGS (50 to 250 µg) were mixed with 2.0 mL of DPPH solution. Each mixture was kept in the dark for 30 min and the absorbance was measured at 517 nm against a blank. Ascorbic acid was used as standard [18]. The inhibition percentage for scavenging DPPH radical was calculated according to the equation.

$\% \text{ DPPH} = (A_0 - A_1 / A_0) \times 100$

2.3 Synthesis of NiNPs of Gloriosa superba tuber (GSNiNPs)

1M Nickel chloride solution and the crude methanolic extract of *Gloriosa superba* tuber (1mg/1ml) mixed in the ratio (1:2 and 1:10). The mixture was heated at 80^{o}C under thorough stirring for 45 minutes until the color changed from pale green to dark green. Then incubate it overnight at room temperature to synthesize the Nickel nanoparticles [19].

2.4 Characterization of GSNiNPs

This phase involved the characterization of GSNiNPs by phytochemicals screening, UV-Visible Spectroscopy, Scanning Electron Microscope (SEM) with Energy Dispersive Spectroscopy (EDX), Dynamic Light Scattering (DLS), Zeta-Potential Fourier Transform Infrared Spectroscopy (FT-IR) and X-RAY Diffraction analysis (XRD), Transmission Electron Microscopy (TEM).

2.5 Characterization of *Gloriosa superba* Nickel nanoparticles

2.5.1Uv-Visible Spectroscopy

To verify the formation of nanoparticles the powder was scanned in the range of 200–800 nm in a spectrophotometer[19].

2.5.2 Scanning Electron Microscopy (SEM)

The size and the morphology of Nickel nanoparticles were examined using SEM. Vacuum dried small amount of prepared Nickel nanoparticles samples was kept on an SEM stub using double-sided adhesive tape at 50mA for 6 min through a sputter. Afterwards, the stub containing the sample was placed in the scanning electron microscopy (SEM) Chamber. The photomicrograph was taken at an acceleration voltage of 20KV [20].

2.5.3 Transmission Electron Microscopy (TEM)

TEM analysis was performed in the FEI Tecnai TEM at an accelerating voltage of 80kV. Samples were prepared by placing drops of nickel nanoparticles suspension over the carbon-coated copper grid, extra

solution was removed by blotting paper and allowing the solvent to evaporate with the help of a critical point drier. An image was formed by the interaction of electrons transmitted through the specimen [21].

2.5.4 Dynamic Light Scattering (DLS)

In this method, a sample solution containing the particles is placed in the path of a monochromatic beam of light and the temporal fluctuations of the scattered light due to the Brownian motion of the particles is determined. This technique involves the calculation of particles size on the basis of the Stokes-Einstein equation [22].

2.5.5 Zeta Potential

The Zeta potential of the nanoparticle was measured by laser Doppler anemometry using a Zetasizer Nano Series (Malvern Instruments, Worcestershire, UK). Nanoparticle samples were diluted in ultrapure MilliQ water and placed in the electrophoretic cell where a potential of ± 150 mV was established. The f potential values were calculated as mean electrophoretic mobility values using Smoluchowski's equation [11].

2.5.6 Fourier Transform Infrared Spectroscopy (FTIR)

A Fourier transform infrared spectrometer was used to evaluate the functional groups linking Nickel nanoparticles and the drug linking to the nanoparticles [12].

2.5.7 X-Ray Diffraction (XRD)

X-ray powder diffraction patterns of Nickel nanoparticles were obtained by a Phillips X-PERT PRO X-ray machine. The X-ray source was Cu K radiation (40 kV, 80 mA). Samples were scanned at a scanning rate of 4° min − 1 [23].

2.6 *In-vitro* anticancer activity of *Gloriosa superba* Nickel nanoparticles

Anti-cancer efficacy of *Gloriosa superba* Ni nanoparticles evaluated against apoptotic related pathway proteins.

2.6.1 Culturing of HeLa cell lines

The human cervical cancer HeLa cell lines were used for the cytotoxicity study of GSNiNPs. HeLa cell lines were obtained from the National Centre for Cell Science (NCCS, Pune, India), were grown in Dulbecco's modified Eagle's medium. This medium was supplemented with 10% FBS and 1% penicillin-streptomycin at 37°*C* under a 5% CO2/ 95% humidified atmosphere [24].

2.6.2 Determination of cell viability using MTT assay.

The monolayer cell culture was trypsinized and the cell count was adjusted to 1×10^4 cells/ml using a medium containing 10% FBS. To each well of the 96 microtiter plate, 0.2 ml of the diluted cell suspension

(~ 10,000 cells) was added. After 24 hours when a partial monolayer was formed, the supernatant was flicked off, wash the monolayer once. Different concentrations of GSNiNPs (10, 50, and 100µg) diluted in media were added and incubated for 2 hours to see the effect of GSNiNPs on the cell viability in a dose-dependent manner. After 2 hours 20 µl of MTT in 200µl was added to each well and incubated for a period of 4 hours at 37˚c. Then MTT was flicked off and 200µl of DMSO was added and mixed thoroughly to dissolve dark blue crystals. After a few minutes, the absorbance was read at 570nm using the ELISA reader [25].Percentage viability was calculated using the formula

% viability = OD of test/ OD of control × 100

2.6.3 Wound healing assay

The inhibition of tumour cell migration by GSNiNPs was performed by wound-healing assay. Briefly, cells were allowed to grow into full confluence in 6-well plates, and then a vertical wound was created with a 200µl pipette tip. The cell debris was removed and a fresh complete medium with the desired concentration of GSNiNPs was added. Cells were incubated at 37°C and 5% CO2 for 24 hours and photographed using a microscope at three-time points (0, 12 and 24hours). The area of migration was measured and analyzed with Image J software [26].

2.6.4 DAPI staining

The occurrence of apoptosis was evaluated by DAPI staining. Cells were seeded and incubated with GSNiNPS for 24hour. Before staining, treated cells were fixed with 3.7% paraformaldehyde for 5 min at room temperature and then washed twice with PBS. DAPI was added to the fixed cells for 5 min, after which they were examined by fluorescence microscopy. Apoptotic cells were identified by condensation and fragmentation of the nuclei. The percentages of apoptotic cells were calculated as the ratio of apoptotic cells to total cell counted ×100. A minimum of 300 cells was counted for each treatment group [24].

2.6.5 Detection of apoptosis by acridine orange and ethidium bromide staining

Cells were seeded and incubated with GSNiNPs for 24 h. The control and treated cells were trypsinized and mixed thoroughly to obtain a single cell suspension. Trypsin was neutralized by the addition of complete medium and 20.0 mL cell suspension was incubated with 10.0 mL 100.0 mg/mL ethidium bromide and 10.0 mL of 100.0 mg/mL acridine orange mixture for 5.0 minutes. The cells were imaged using the fluorescence microscope [27].

2.6.6 Anticancer efficacy of GSNiNPs against the apoptotic related genome expression in Cervical Cancer-Gene expression

Cells were seeded and incubated with GSNiNPs for 24 hours. RNA was isolated from the cells treated with GSNiNPs by using RNeasy mini kit method and the quantity and purity of the RNA isolated was

determined by nanodrop spectrophotometer. The RNA isolated was converted into cDNA and RT PCR was performed using prime script RT PCR kit for measuring the expression of four genes (β actin, VEGF A and B, caspase3 and caspase9). After the amplification was done the PCR products were separated by agarose gel electrophoresis [28]. Sequences of the primers used in RT-PCR are listed in Table 1.

Table 1
List of primers used

GENES	SEQUENCE (5'-3')	Length (bp)
β actin FP	GTGGGGCGCCCCAGGCACCA	20
β actin RP	CTTCCTTAATGTCACGCACGATTTC	25
VEGF A FP	GCAGAATCATCACGAAGTGG	20
VEGF A RP	GCATGGTGATGTTGGACTCC	20
Casp-3 FP	TGTGAGGCGGTTGTAGAAGA	20
Casp-3 RP	TGTGAGGCGGTTGTAGAAGA	20
Casp-9 FP	TGCTGAGCAGCGAGCTGTT	19
Casp-9 RP	AGCCTGCCCGCTGGAT	16
VEGF B FP	CCTTGACTGTGGAGCTCATG	20
VEGF B RP	TGTCTGGCTTCACAGCACTG	20

The sequence of primers used in RT-PCR analysis for determining the mRNA expression of genes (β actin, caspase3 and caspase9) and gene involved in angiogenesis (VEGF A and VEGF B) in GSNiNPs treated cells compared with the control cells.

3. Results

3.1 Diphenyl-1-picrylhydrazyl (DPPH) radical scavenging activity of methanolic extract of *Gloriosa superba*.

The free radical scavenging effect of MEGS was evaluated using the DPPH radical assay. From the result of the DPPH assay, the IC50 value of MEGS was obtained as 70.67μg/ml (Fig. 1). The results showed that the MEGS has high antioxidant potency due to the bioactive compounds present in the methanolic extract.

3.2 Synthesis of GSNiNP*s*

The synthesis of GSNiNPs was confirmed by observing the colour change from yellowish green to dark green after overnight incubation (Fig. 2). The pH of nickel chloride solution was found to be 4.0, when we

add MEGS to this nickel chloride solution, pH changes from 4.0 to 5. The actual pH of MEGS was 6. This, confirmed that capping between nickel and MEGS were taken place. And the formation of GSNiNPs was further confirmed by UV Spectroscopy and SEM.

3.3 Characterization of GSNiNPs

The above synthesized GSNiNPs were subjected to various characterization techniques such as UV spectrum analysis, SEM, TEM, DLS, zeta potential, FTIR and XRD.

3.3.1 UV-Visible Spectrum analysis of GSNiNPs

The absorption peak of GSNiNPs has been studied with the help of UV–Visible spectroscopy at various time intervals. The absorbance was recorded from 200 to 800 nm. The obtained results depicted the prominent peak at 350 nm (Fig. 3) which indicates the conversion of nickel salt solution to nickel nanoparticles by the reduction of bioactive compounds of *Gloriosa superba* towards metal salts. This clearly indicated the interaction between the metal nickel and bio-molecules present in the extract and the remarkable broadening of peak indicated that the particles are highly polydispersed.

3.3.2 SEM analysis of GSNiNPs

The size and the surface morphology of the GSNiNPs were determined by SEM and the elemental composition of the GSNiNPs was further confirmed by the Energy Dispersive X-ray (EDX) analysis. The SEM image of GSNiNPs was found to be agglomerated with the particle size ranges from 521.54nm to 843.80nm (Fig. 4a). The EDX spectrum reveals the presence of few traces of oxygen found in Nickel chloride (Fig. 4b).

3.3.3 TEM analysis of GSNiNPs

The TEM image of the GSNiNPs (Fig. 5) showed that the particles are spherical in shape. The diameter of the sample size ranges between 19 and 45 nm and shows a certain extent of particles agglomeration. The result obtained was found to be correlated with the size of the nanoparticles calculated using SEM analysis.

3.3.4 DLS analysis of GSNiNPs

DLS measures the hydrodynamic diameter of the particle, plus ions or molecules that are attached to the surface and move with the NiNPs in solution [18]. DLS studies of biosynthesized GSNiNPs showed variable but gradual changes in the particle size based on the increase in molar concentration of the stock solution. The size distribution graph shows the average size of the synthesized GSNiNPs to be approximately 143.1 nm with a low polydispersity index (Fig. 6). Slight variation in the peak absorbance was observed which might be due to variation in particle size distribution which was further confirmed with DLS.

3.3.5 Zeta potential analysis of GSNiNPs

Zeta potential analysis revealed that the GSNiNPs possessed a positive surface charge which indicates that the nanoparticles get aggregated. The Zeta potential analysis of GSNiNPs demonstrated that it has positive charges of 0.979 mV (Fig. 7). These outcomes indicated that the plant Gloriosa superba was a good source for the reduction of narrow sized GSNiNPs. The positive zeta potential value confirmed synthesized nanoparticles have higher stability in the suspension medium.

3.3.6 FTIR analysis of GSNiNPs

FTIR analysis results revealed the functional groups present in GSNiNPs. The functional groups are responsible for the reduction and capping of GSNiNPs. The peaks obtained in FTIR are 3471.24 cm-1 (O–H stretching), 3388.35 cm-1 (C–C stretching), 2165.67 cm-1 (C–C stretching), 1619.91 cm-1 (C–N stretching), 600.314 cm-1 (O–H stretching), 713.533 cm-1(C–N stretching) and 400 cm-1(C–H stretching). The respective peaks correspond to various functional groups like carboxylic acids, primary amines, aromatic hydrocarbons, aliphatic amines and alkanes. The FTIR spectral analysis confirms that the presence of N–H, C–N, C–H and O–H functional groups in the plant extract was responsible for effective stabilization and reduction of nickel nanoparticles. The results obtained were correlated with the results of UV visible spectroscopic analysis.

3.3.7 XRD Analysis of GSNiNPs

The XRD pattern of the biosynthesized GSNiNPs shows three diffraction peaks at 2θ= 20.4500, 16.0795 and 32.9591(Fig. 9). These major peaks reflect the patterns of the face centred cubic and crystalline structure of the biosynthesized GSNiNPs. The average crystalline size of the NPs was determined by using the Scherrer equation. After subjecting the 2θ values in the Scherrer equation, the average crystalline size of GSNiNPs was found to be 37.68 nm.

3.4 In-vitro **anticancer activity of GSNiNPs**

3.4.1 MTT assay

The cytotoxicity activity of GSNiNPs on HeLa cell lines was assessed using MTT assay. The result indicated that GSNiNPs shows significant cytotoxicity activity by decreasing the viability of the cells in a dose and time-dependent manner. The result revealed that the IC_{50} value of the GSNiNPs was found to be 38.85µg/ml (Fig. 10).

3.4.2 Wound healing assay

In order to evaluate the effectiveness of the GSNiNPs on metastasis of cancer cells, it was evaluated using the wound healing assay against HeLa cell lines. The anti-metastatic effect of the GSNiNPs against the HeLa cell lines was evaluated and its migration efficacy was analyzed at 0 hours and 24 hours of incubation. The results revealed that GSNiNPs have the capacity to inhibit the migration and invasion of the cells. From the results, it revealed that wound scratch in untreated cells (control) was started to close after 24 hours of incubation, whereas GSNiNPs co-treated group suppressed the effect of migration of HeLa cell lines (Fig. 11).

3.4.3 DAPI staining

GSNiNPs induced apoptosis and inhibited the angiogenesis in HeLa cells, with the marked morphological nuclear changes were analyzed using DAPI staining. There is a significant number of changes in cells morphology with chromatin condensation and nuclear fragmentation were observed compared to the untreated control.

The extract induced morphological changes which includes cell shrinkage, rounding of cells and membrane blebbing which depicts the induction of apoptosis in HeLa cell lines as shown in (Fig. 12b). It was noted that the number of cells showed the signs of apoptosis (the cells that have brightly fluorescence and fragmented nucleus) in the extract-treated group (IC_{50} value 38.85 µg/ml) when compared to the control group.

3.4.4 Detection of apoptosis by Acridine orange and Ethidium bromide double staining

Apoptosis is an important biochemical process that eliminates the abnormal cells from our body. The ability to induce apoptosis by GSNiNPs in HeLa cell lines was detected using AO-EB dual staining technique. The results indicated that HeLa cell lines undergo apoptosis after 24 hours of treatment with GSNiNPs. GSNiNPs treated cells undergo late apoptosis with nuclear and chromatin condensation or fragmented chromatids (Fig. 13b). Moreover, it was reported that there is a reduction in the number of cells and changes in cell morphology after treatment with GSNiNPs when compared to control cells (Fig. 13a).

3.4.5 Reverse Transcriptase PCR (RT- PCR) analysis

Overexpression of VEGF A and B has been demonstrated to promote cell proliferation and inhibit cell apoptosis in various types of cancer. In our result, we evaluated the inhibitory effect of GSNiNPs on VEGF A and B expression and induction of caspase 3 and 9 in HeLa cell lines. As shown in (Fig. 14) the expression of VEGF A and B were relatively higher in HeLa cells. Further GSNiNPs treated cells significantly down-regulate the expression of VEGF A and B and up-regulate caspase 3 and 9 at mRNA levels in a dose-dependent manner in HeLa cell lines (Fig. 15).

4. Discussion

The methanolic extract of *Gloriosa superba* tuber was subjected to evaluate the free radical scavenging activity (antioxidant) by using DPPH radical. The results obtained shows, GSNiNPs show enhanced antioxidant potency by the presence of bio active compounds present in the extract. Surface reaction phenomenon of these biosynthesized nanoparticles (due to adsorbed antioxidant moiety onto the surface) and high surface area to volume ratio of nanoparticles generate a tendency to interact and scavenged the free radical. The above result was supported by copper oxide nanoparticles at 517 nm [29]. The primary confirmation for nickel nanoparticle was due to colour changes and UV/Vis absorption

spectra of GSNiNPs formed peak at 350 nm and then SEM study was identified that the shape of GSNiNPs appeared slightly spherical shape with rough surface.

GSNiNPs were synthesized using methanolic extract of *Gloriosa superba* tuber and synthesized GSNiNPs were subjected to characterization by using UV Visible spectroscopy, SEM, TEM, DLS, Zeta potential, FTIR and XRD analysis.

UV Visible Spectroscopic analysis of GSNiNPs showed a peak at 350 nm, indicating the interaction between the metal nickel and bio-molecules present in the extract. The remarkable broadening of the peak indicated that the particles are highly polydispersed. The above result was supported by UV Visible absorption peak at 374 nm to 422 nm for *Ocimum sanctum* nickel nanoparticles [19] and 252 nm for *Cocusnucifera* nickel nanoparticles [30].

The SEM image of GSNiNPs revealed the formation of slightly spherical and agglomerated nanoparticles. The agglomeration of GSNiNPs may be due to the presence of magnetic interaction between the particles. The EDAX analysis indicated the presence of Nickel, chloride and oxygen elements present in the GSNiNPs. The result obtained has been supported by the SEM result of silver nanoparticles [20].

The TEM image of the GSNiNPs revealed that the spherical shape of the particles and the distribution of the particles are narrow. The agglomeration property of the nanoparticles is due to magnetic interaction and polymer adherence between the particles. The TEM result was supported by[21] reported the agglomeration of TiO2 nanoparticles.

The hydrodynamic particle size distribution and polydispersity index of the biosynthesized GSNiNPs were measured using the DLS technique. The hydrodynamic size includes the hydration layer and the surface of NiNPs, thus the results of DLS was correlated with the results of SEM images. The phytochemicals in the plant extract may contribute to the hydrodynamic size. This result is supported by the DLS analysis of *A. paniculata* AgNPs showed an average particle size of 68.06 nm [22].

Zeta potential (ζ) analysis revealed that the GSNiNPs have a positive surface charge. Zeta potential value represents the charge of the nanoparticle and indicates the interaction between them in the colloidal system. All the GSNiNPs in the suspension are positively charged particles, so they tend to repel each other without aggregation [31]. Similar results were obtained by [11] in which the zeta potential value of *Sygyziumcumini* silver Nanoparticle was found to be 19.6 mV.

FTIR confirmed the vibrational stretching modes of metal-oxygen bonds in GSNiNPs. FT-IR studies clearly showed the formation of GSNiNPs and indicated that the plant extract contains various phytochemicals, which work as a capping and stabilizing agent for the reduction of nickel to nickel nanoparticles. The prominent peaks of iron oxide nanoparticles have been reported previously with a small difference in the respective wave number [12].

XRD analysis of GSNiNPs confirmed the presence of crystalline structure. This pattern of the crystalline structure of nickel nanoparticles of *Gloriosa superba* is responsible to inhibit the proliferation,

angiogenesis and inducing apoptosis in HeLa cell lines. The peaks at different degrees have been previously reported and the morphology, nanocrystalline size of AgNPs were determined [23].

In vitro anticancer effect of GSNiNPs was evaluated using various methods. MTT assay was performed to evaluate the effect of GSNiNPs on the proliferation of HeLa cell lines. The GSNiNPs possess dose and time-dependent cytotoxicity against HeLa cell lines. Our results demonstrated that GSNiNPs significantly inhibits proliferation, angiogenesis and induce apoptosis in HeLa cell lines. The result was supported by Li et al., (2011), which reported that Oroxin B decreases the expression of COX-2/VEGF and PTEN/Pl3K/AKT in liver cancer [25]. Due to the presence of tight interendothelial junctions, the drug particles could not penetrate the healthy cells. However, in tumour tissues, the gap between the endothelial junctions will increase, and nanoparticles can easily penetrate to cancer cite through extravasation. Target specific drug deliveries depend on certain factors by either endogenous (pH, redox, enzyme) or exogenous (temperature, acoustic, light). Using carriers for drug delivery will improve the circulation time, site-specific delivery, solubility of drugs, and permeability. Nickel is considered a good adsorbent due to its chemical and magnetic properties. On exposure to the magnetic field, NiNPs will generate heat, which helps the drug delivery.

The GSNiNPs induced apoptosis and anti-angiogenesis were examined by DAPI staining. Analyzing the morphological changes of HeLa cells after GSNiNPs treatment confirms the signs of drug-induced apoptosis. The results demonstrated that a significant number of GSNiNPs treated HeLa cells with chromatin condensation and nuclear fragmentation when compared to the untreated cells. The apoptotic cells are shown as the fragmented nucleus which emits bright fluorescence. This was supported by the induction of apoptosis by green synthesized gold nanoparticles by the activation of caspase-3 and 9 in human cervical cancer cells [24].

In order to evaluate the effectiveness of the GSNiNPs on metastasis of cancer cells using wound healing assay in HeLa cell lines. Wound healing assay results indicated that cell migration and invasion inhibitory effect of GSNiNPs in HeLa cells. This effect may be due to the activation of caspase 3 and 9 and the reduction of VEGF A and VEGF B in HeLa cells. The results indicated that GSNiNPs treated group showed closing of the gap after 24 hours of incubation compared to the control group, revealing the inhibition of migration in HeLa cell lines. This result was supported by induction of apoptosis and inhibition of invasion in gastric cancer cells by TiO2 nanoparticles [26].

Dual AO/EB fluorescent staining can detect basic morphological changes in apoptotic cells. In addition, it allows for the distinction between normal, early and late apoptotic, and necrosis in cells. Therefore, in AO/EB staining the live cells were green, the cells undergoing late and early were yellow and reddish-orange respectively. This is a qualitative and quantitative method to detect apoptosis. Moreover, it was reported that there is a reduction in the number of cells and changes in cell morphology after treatment with GSNiNPs compared to control cells after 24 hours of incubation. This result was supported by the DNA in HEP 2 cells becoming as dense, fragmented and condensed chromatin after being treated with *Crotalaria verucosa* ZnO nanoparticles [27].

Based on the RT- PCR results we hypothesis that GSNiNPs could decrease VEGF A and B transcription by increasing the apoptotic levels of caspase 3 and 9 to induce cell death in HeLa cell lines. This result suggested that the inhibitory effect of GSNiNPs on the proliferation of HeLa cells is mediated by regulating the activity of VEGF A and B signalling. This result was supported by the anti-cancer activity of curcumin loaded nanoparticles in prostate cancer [28].

5. Conclusion

In this study, green synthesis of GSNiNPs using the methanolic extracts of *Gloriosa superba* tuber was done and characterized using UV–Visible spectrum, SEM, TEM, DLS, FT-IR, zeta potential and XRD analysis. The synthesized GSNiNPs showed potent anti-cancer and anti-angiogenic activity against cervical cancer was explored using MTT, wound healing, DAPI and Double staining techniques. The anti-angiogenic activity of GSNiNPs against HeLa cell lines was induced by an increase in the expression levels of caspase 3 and 9 and a decrease in VEGF A and B. Overall findings revealed that the GSNiNPs can act as an effective anti-cancer therapeutic agent for cervical cancer. In this regard, the GSNiNPs brought a new approach to improve the bioavailability of drug-responsive for the treatment of cervical cancer.

Abbreviations

GSNiNPs- *Gloriosa superba* nickel nanoparticles

MEGS- Methanolic extract of *Gloriosa superba*

SEM- Scanning Electron Microscopy

EDX- Energy Dispersive X-ray

TEM-Transmission Electron microscopy

DLS- Dynamic Light Scattering

FTIR- Fourier Transform Infrared Spectrometer

XRD- X-ray Diffraction

RT-PCR- Reverse Transcriptase- PCR

Declarations

- **Conflict of Interest**: The authors declare that they have no conflict of interest.
- **Ethical approval**: For this type of study, formal consent is not required.

- **Consent to participate**: Informed consent was obtained from all individual participants involved in the study.
- **Consent for publication**: All individual participants involved in the study reach a consensus on the publication of this manuscript.
- **Availability of data and materials**: Data sharing is not applicable to this article as no datasets were generated or analyzed during the current study.
- **Authors' contributions**:

Mrudhulla S: Drafting the article and submitting the final version of the article

Anjali K Ravi: Drafting the article and submitting the final version of the article.

Saradhadevi Muthukrishnan: Corresponding author make sustainable contribution for the intellectual input and designing the whole paper

Velayuthaprabhu Shanmugam: Co-author who might assist the corresponding author and first author in writing the article.

VijayaAnandArumugam: Co-author who might assist the corresponding author and first author in writing the article.

Arun Muthukrishnan: Co-author who might assist the corresponding author and first author in writing the article.

References

[1] R. L. Siegel, K. D. Miller, and A. Jemal, “Cancer statistics, 2019,” *CA. Cancer J. Clin.*, vol. 69, no. 1, pp. 7–34, Jan. 2019, doi: 10.3322/caac.21551.

[2] F. Bray, J. Ferlay, I. Soerjomataram, R. L. Siegel, L. A. Torre, and A. Jemal, “Global cancer statistics 2018: GLOBOCAN estimates of incidence and mortality worldwide for 36 cancers in 185 countries,” *CA. Cancer J. Clin.*, vol. 68, no. 6, pp. 394–424, Nov. 2018, doi: 10.3322/caac.21492.

[3] M. Schiffman, P. E. Castle, J. Jeronimo, A. C. Rodriguez, and S. Wacholder, “Human papillomavirus and cervical cancer,” *Lancet*, vol. 370, no. 9590, pp. 890–907, Sep. 2007, doi: 10.1016/S0140-6736(07)61416-0.

[4] A. R. Kreimer *et al.*, “Evidence for single-dose protection by the bivalent HPV vaccine—Review of the Costa Rica HPV vaccine trial and future research studies,” *Vaccine*, vol. 36, no. 32, pp. 4774–4782, Aug. 2018, doi: 10.1016/j.vaccine.2017.12.078.

[5] L. Y. Pang, E. A. Hurst, and D. J. Argyle, “Cyclooxygenase-2: A Role in Cancer Stem Cell Survival and Repopulation of Cancer Cells during Therapy,” *Stem Cells Int.*, vol. 2016, pp. 1–11, 2016, doi:

10.1155/2016/2048731.

[6] M. S. Gordon, “Vascular endothelial growth factor as a target for antiangiogenic therapy,” *J. Clin. Oncol.*, vol. 18, no. 21 SUPPL., pp. 2–10, 2000.

[7] X. Li, “Novel VEGF family members: VEGF-B, VEGF-C and VEGF-D,” *Int. J. Biochem. Cell Biol.*, vol. 33, no. 4, pp. 421–426, Apr. 2001, doi: 10.1016/S1357-2725(01)00027-9.

[8] M. Ferrari, “Cancer nanotechnology: opportunities and challenges,” *Nat. Rev. Cancer*, vol. 5, no. 3, pp. 161–171, Mar. 2005, doi: 10.1038/nrc1566.

[9] K. M. Annapoorani, S, Saradha Devi, “Antioxidant and antitumorigenic efficacy of methanolic extracts of gloriosa superba and silver nanoparticles of methanolic extracts of gloriosa superba to dla tumor cells,” 2014.

[10] B. A. Vaishnavi, H. Khanm, and H. R. Bhoomika, “Review on Pharmacological Properties of Glory Lily (Gloriosa superba Linn.): An Endangered Medicinal Plant,” *Int. J. Curr. Microbiol. Appl. Sci.*, vol. 8, no. 02, pp. 1359–1364, 2019, doi: 10.20546/ijcmas.2019.802.159.

[11] N. Atale, S. Saxena, J. G. Nirmala, R. Narendhirakannan, S. Mohanty, and V. Rani, “Synthesis and Characterization of Sygyzium cumini Nanoparticles for Its Protective Potential in High Glucose-Induced Cardiac Stress: a Green Approach,” *Appl. Biochem. Biotechnol.*, vol. 181, no. 3, pp. 1140–1154, Mar. 2017, doi: 10.1007/s12010-016-2274-6.

[12] N. Modanlou Juibari and A. Eslami, “Synthesis of nickel oxide nanorods by Aloe vera leaf extract,” *J. Therm. Anal. Calorim.*, vol. 136, no. 2, pp. 913–923, Apr. 2019, doi: 10.1007/s10973-018-7640-x.

[13] D.-H. Chen and C.-H. Hsieh, “Synthesis of nickel nanoparticles in aqueous cationic surfactant solutions,” *J. Mater. Chem.*, vol. 12, no. 8, pp. 2412–2415, Jul. 2002, doi: 10.1039/b200603k.

[14] D. Guo, C. Wu, X. Li, H. Jiang, X. Wang, and B. Chen, “In Vitro Cellular Uptake and Cytotoxic Effect of Functionalized Nickel Nanoparticles on Leukemia Cancer Cells,” *J. Nanosci. Nanotechnol.*, vol. 8, no. 5, pp. 2301–2307, May 2008, doi: 10.1166/jnn.2008.18272.

[15] A. A. Ezhilarasi, J. J. Vijaya, K. Kaviyarasu, M. Maaza, A. Ayeshamariam, and L. J. Kennedy, “Green synthesis of NiO nanoparticles using Moringa oleifera extract and their biomedical applications: Cytotoxicity effect of nanoparticles against HT-29 cancer cells,” *J. Photochem. Photobiol. B Biol.*, vol. 164, pp. 352–360, Nov. 2016, doi: 10.1016/j.jphotobiol.2016.10.003.

[16] N.-D. Jaji, H. L. Lee, M. H. Hussin, H. M. Akil, M. R. Zakaria, and M. B. H. Othman, “Advanced nickel nanoparticles technology: From synthesis to applications,” *Nanotechnol. Rev.*, vol. 9, no. 1, pp. 1456–1480, Dec. 2020, doi: 10.1515/ntrev-2020-0109.

[17] H. R. El-Seedi *et al.*, “Metal nanoparticles fabricated by green chemistry using natural extracts: biosynthesis, mechanisms, and applications,” *RSC Adv.*, vol. 9, no. 42, pp. 24539–24559, 2019, doi: 10.1039/C9RA02225B.

[18] S. N. Kharat and V. D. Mendhulkar, “‘Synthesis, characterization and studies on antioxidant activity of silver nanoparticles using Elephantopus scaber leaf extract,’” *Mater. Sci. Eng. C*, vol. 62, pp. 719–724, May 2016, doi: 10.1016/j.msec.2016.02.024.

[19] C. J. Pandian, R. Palanivel, and S. Dhananasekaran, “Green synthesis of nickel nanoparticles using Ocimum sanctum and their application in dye and pollutant adsorption,” *Chinese J. Chem. Eng.*, vol. 23, no. 8, pp. 1307–1315, Aug. 2015, doi: 10.1016/j.cjche.2015.05.012.

[20] A. Haider *et al.*, “A novel use of cellulose based filter paper containing silver nanoparticles for its potential application as wound dressing agent,” *Int. J. Biol. Macromol.*, vol. 108, pp. 455–461, Mar. 2018, doi: 10.1016/j.ijbiomac.2017.12.022.

[21] J. Wang *et al.*, “Time-dependent translocation and potential impairment on central nervous system by intranasally instilled TiO2 nanoparticles,” *Toxicology*, vol. 254, no. 1–2, pp. 82–90, Dec. 2008, doi: 10.1016/j.tox.2008.09.014.

[22] V. Sharma, S. Kaushik, P. Pandit, D. Dhull, J. P. Yadav, and S. Kaushik, “Green synthesis of silver nanoparticles from medicinal plants and evaluation of their antiviral potential against chikungunya virus,” *Appl. Microbiol. Biotechnol.*, vol. 103, no. 2, pp. 881–891, Jan. 2019, doi: 10.1007/s00253-018-9488-1.

[23] S. O. Aisida *et al.*, “Biosynthesis of silver oxide nanoparticles using leave extract of Telfairia Occidentalis and its antibacterial activity,” *Mater. Today Proc.*, vol. 36, pp. 208–213, 2021, doi: 10.1016/j.matpr.2020.03.005.

[24] J. Baharara, T. Ramezani, A. Divsalar, M. Mousavi, and A. Seyedarabi, “Induction of Apoptosis by Green Synthesized Gold Nanoparticles Through Activation of Caspase-3 and 9 in Human Cervical Cancer Cells.,” *Avicenna J. Med. Biotechnol.*, vol. 8, no. 2, pp. 75–83, [Online]. Available: http://www.ncbi.nlm.nih.gov/pubmed/27141266.

[25] X. Li, H. Xu, Z.-S. Chen, and G. Chen, “Biosynthesis of Nanoparticles by Microorganisms and Their Applications,” *J. Nanomater.*, vol. 2011, pp. 1–16, 2011, doi: 10.1155/2011/270974.

[26] M. Nasr, C. Eid, R. Habchi, P. Miele, and M. Bechelany, “Recent Progress on Titanium Dioxide Nanomaterials for Photocatalytic Applications,” *ChemSusChem*, vol. 11, no. 18, pp. 3023–3047, Sep. 2018, doi: 10.1002/cssc.201800874.

[27] S. S. Sana *et al.*, “Crotalaria verrucosa Leaf Extract Mediated Synthesis of Zinc Oxide Nanoparticles: Assessment of Antimicrobial and Anticancer Activity,” *Molecules*, vol. 25, no. 21, p. 4896,

Oct. 2020, doi: 10.3390/molecules25214896.

[28] M. M. Yallapu *et al.*, “Anti-cancer activity of curcumin loaded nanoparticles in prostate cancer,” *Biomaterials*, vol. 35, no. 30, pp. 8635–8648, Oct. 2014, doi: 10.1016/j.biomaterials.2014.06.040.

[29] D. Das, B. C. Nath, P. Phukon, and S. K. Dolui, “Synthesis and evaluation of antioxidant and antibacterial behavior of CuO nanoparticles,” *Colloids Surfaces B Biointerfaces*, vol. 101, pp. 430–433, Jan. 2013, doi: 10.1016/j.colsurfb.2012.07.002.

[30] G. Elango, S. M. Roopan, K. I. Dhamodaran, K. Elumalai, N. A. Al-Dhabi, and M. V. Arasu, “Spectroscopic investigation of biosynthesized nickel nanoparticles and its larvicidal, pesticidal activities,” *J. Photochem. Photobiol. B Biol.*, vol. 162, pp. 162–167, Sep. 2016, doi: 10.1016/j.jphotobiol.2016.06.045.

[31] S. Singh, A. Bharti, and V. K. Meena, “Structural, thermal, zeta potential and electrical properties of disaccharide reduced silver nanoparticles,” *J. Mater. Sci. Mater. Electron.*, vol. 25, no. 9, pp. 3747–3752, Sep. 2014, doi: 10.1007/s10854-014-2085-x.

Figures

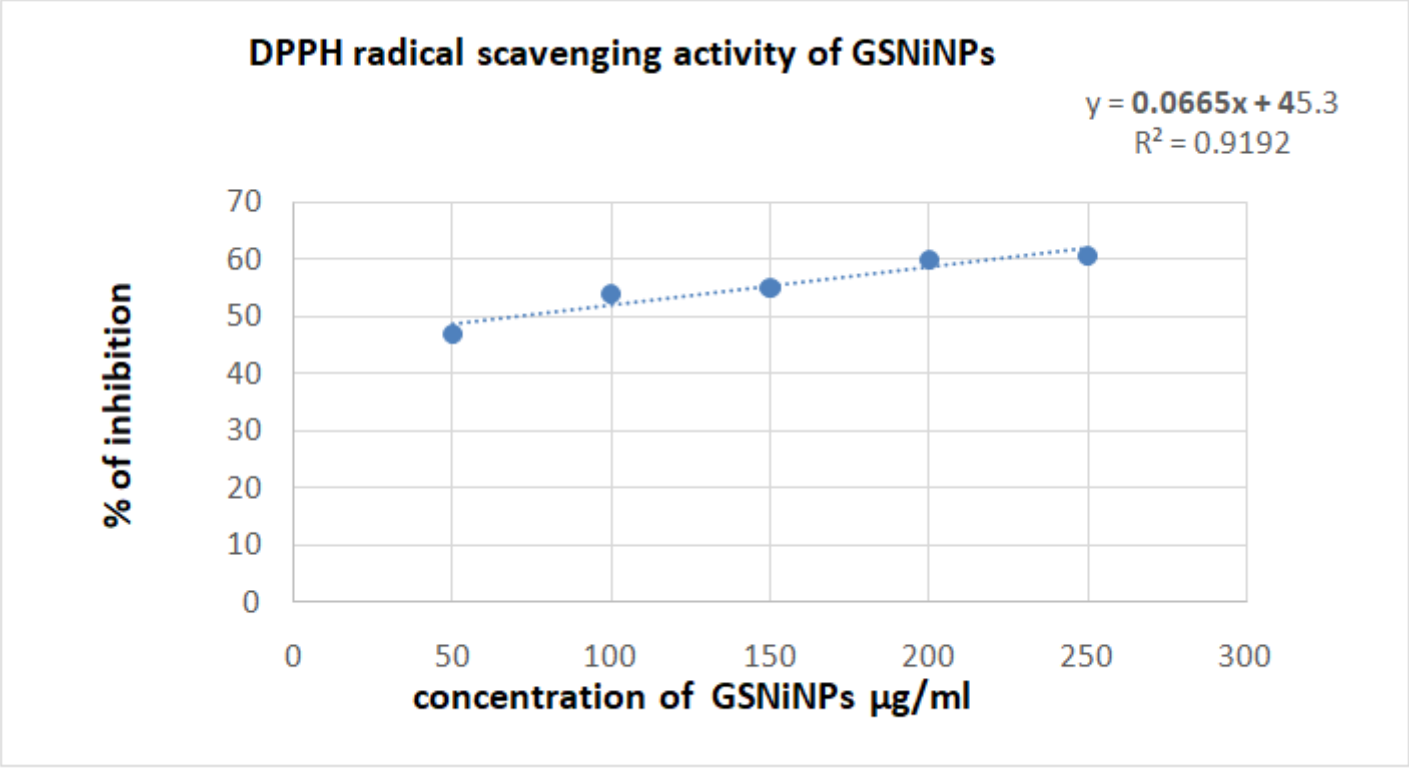

Figure 1

DPPH radical scavenging activity of GSNiNPs: Graph represents the DPPH radical scavenging activity of **GSNiNPs**at various concentrations**.**

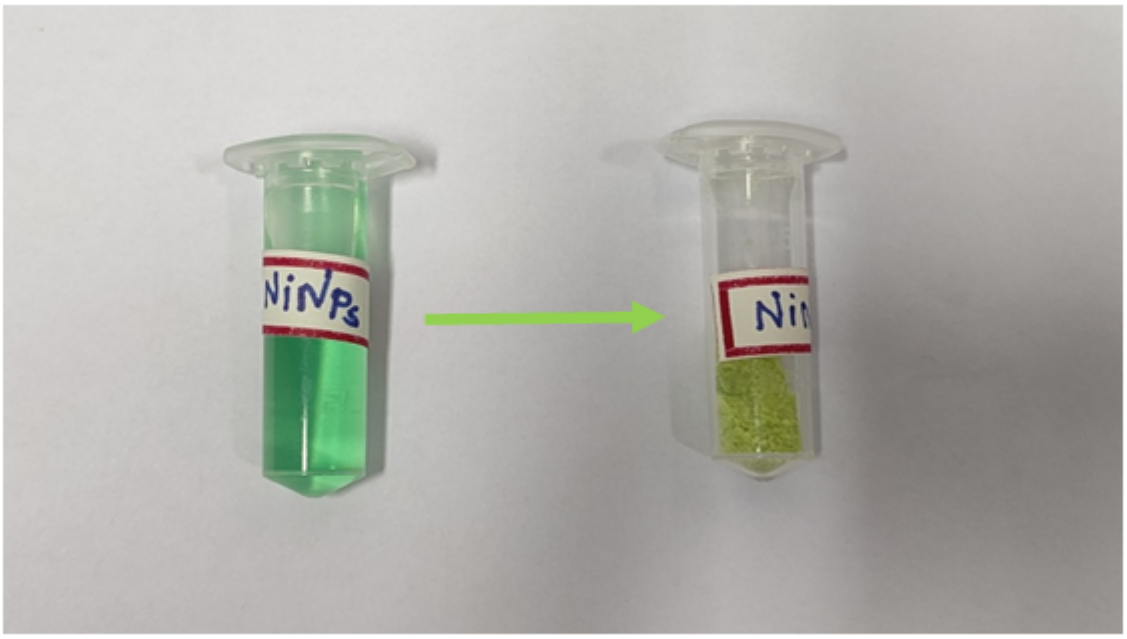

Figure 2

Nickel Nanoparticles of *Gloriosa superba:* Green synthesis of **GSNiNPs**, Nickel chloride was used as a precursor. 1M Nickel chloride solution and the crude methanolic extract of *Gloriosa superba* tuber (1mg/1ml) mixed in the ratio (1:2 and 1:10). The mixture was heated at 80^{o}C under thorough stirring for 45 minutes until the color changed from pale green to dark green.

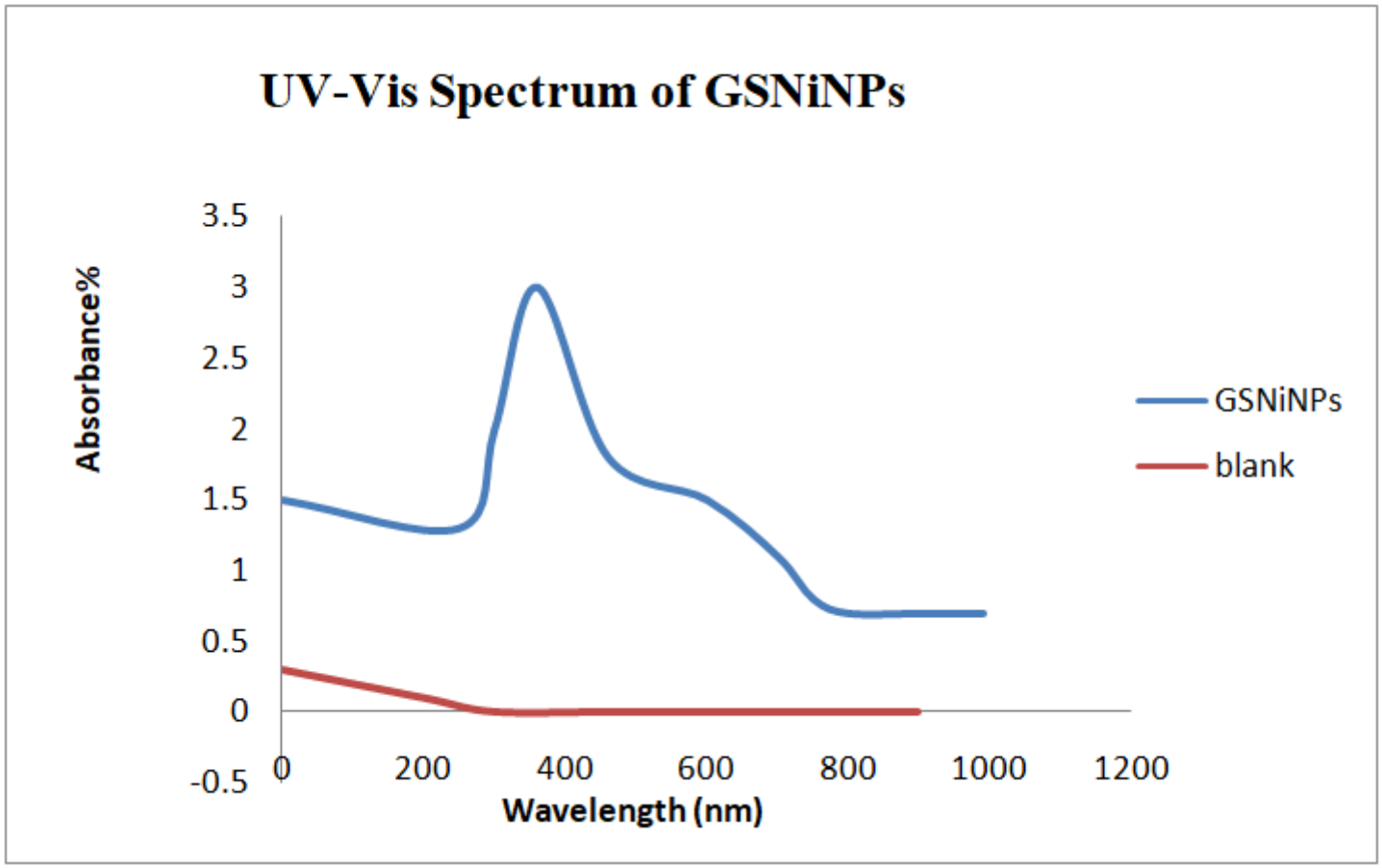

Figure 3

UV Visible spectroscopy of GSNiNPs: UV-visible spectrum analysis of **GSNiNPs** shows a prominent peak at 350 nm.

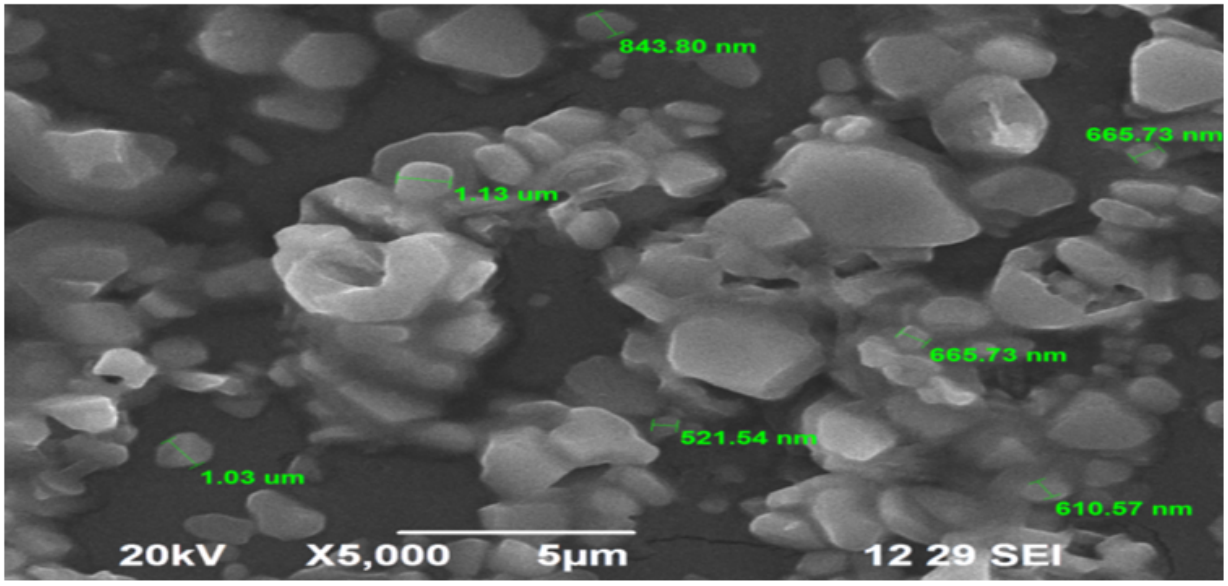

(A)

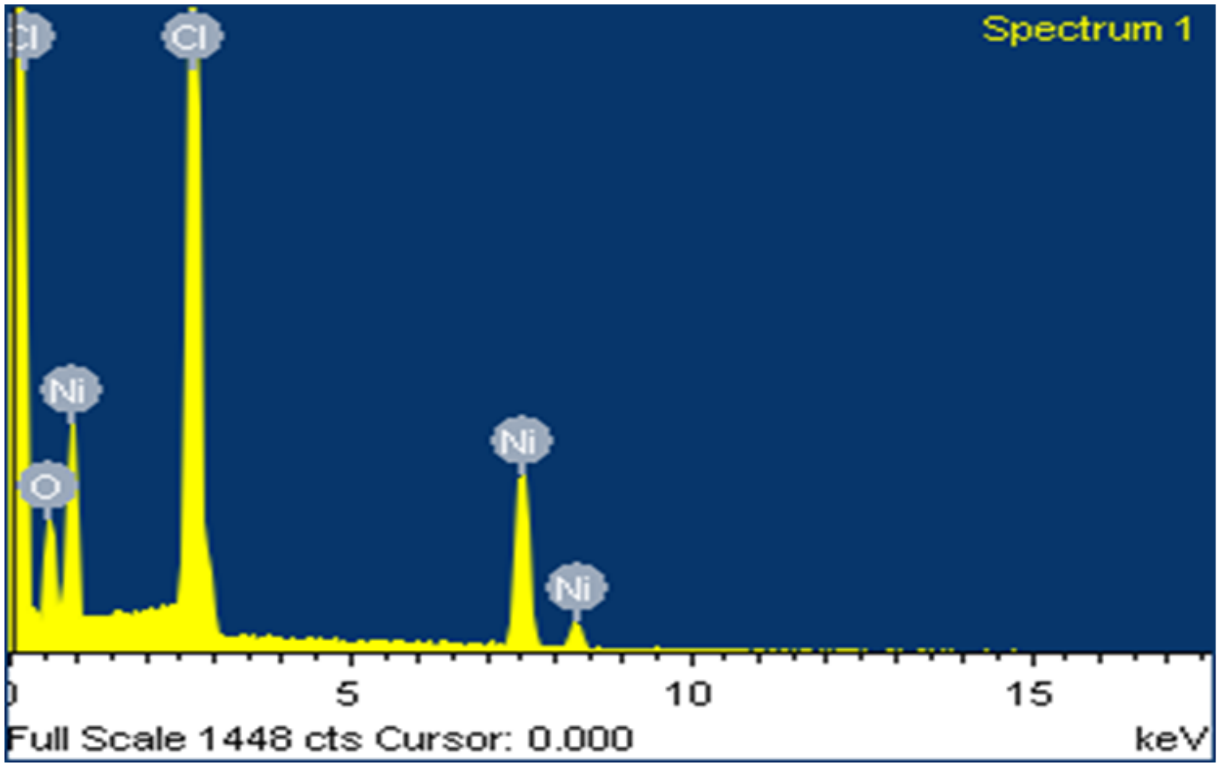

(B)

Figure 4

(A) SEM analysis of GSNiNPs:The size and morphology of green synthesized GSNiNPs wereanalyzed using SEM. SEM image revealed that the average particle size of GSNiNPs ranged from 521.54nm to 843.80nm.

(B): EDX spectrum of GSNiNPs: The elemnetal composition of GSNiNPs were confirmed using EDX analysis. The EDX spectrum reveals the presence of few traces of oxygen found in Nickel chloride

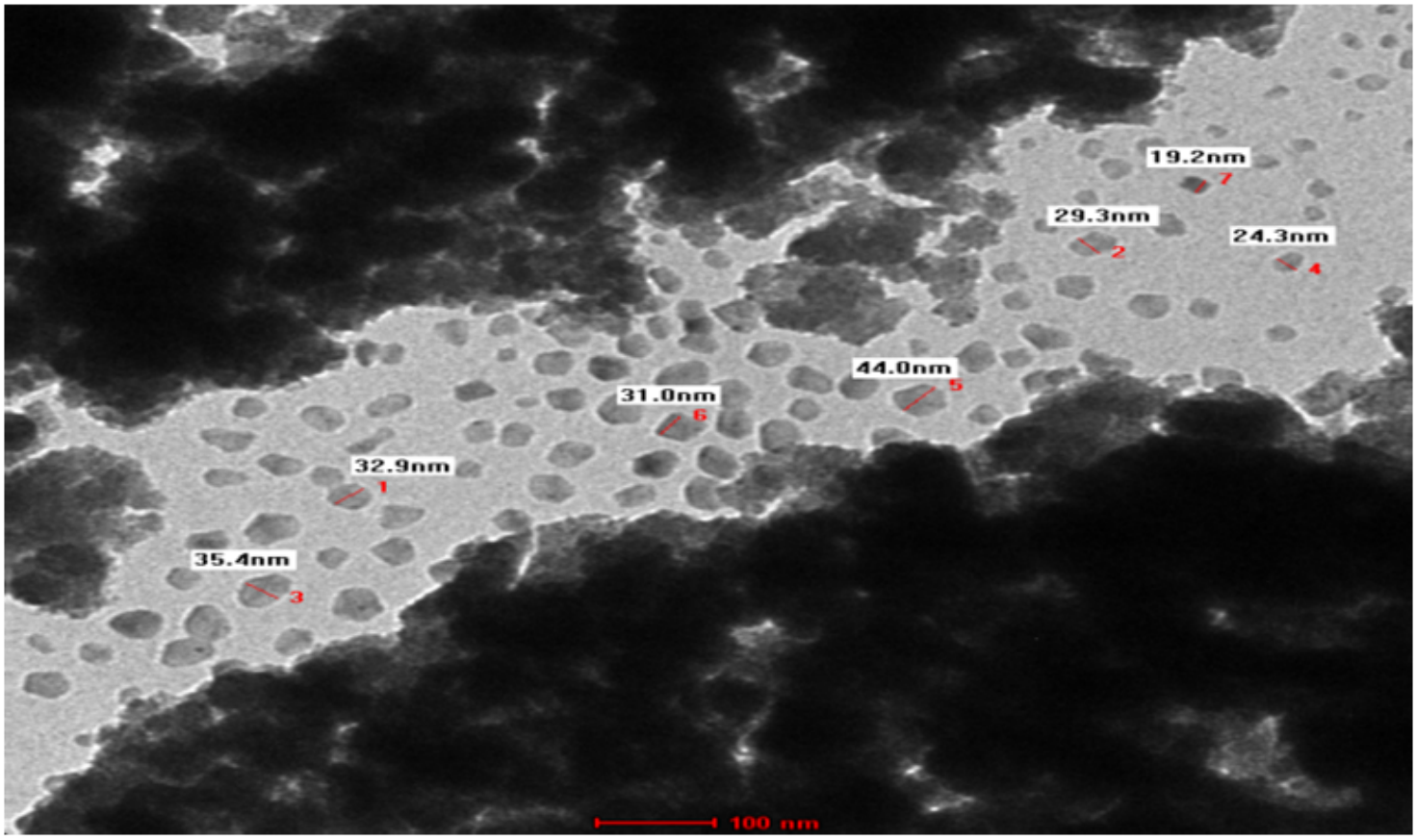

Figure 5

TEM Image of GSNiNPs: The TEM image of the GSNiNPsrevealed that the particles are spherical in shape with sample size ranges between 19 and 45 nm.

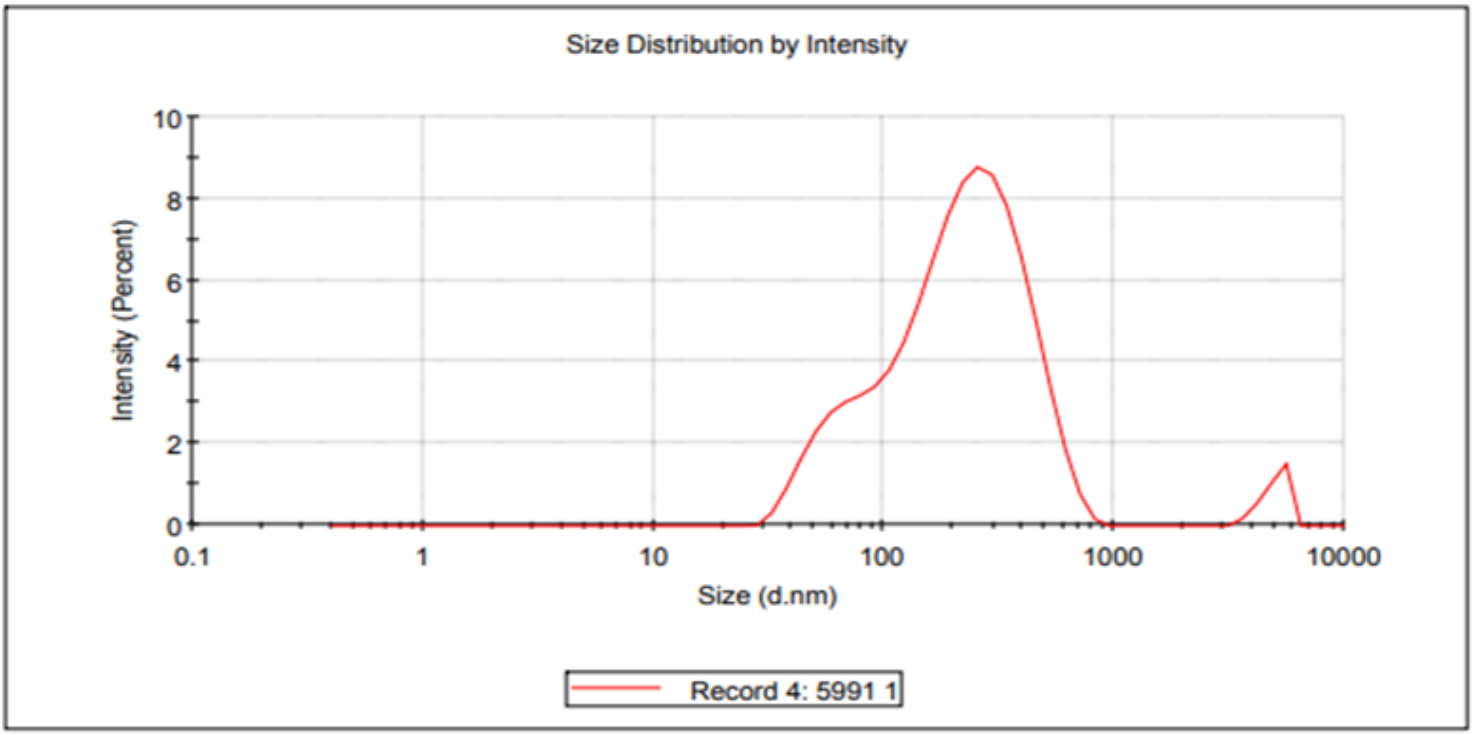

Figure 6

DLS histogram of GSNiNPs: The average particle size distribution of **GSNiNPs** was analyzed using DLS analysis. The size distribution graph shows the average size of the synthesized GSNiNPs to be approximately 143.1 nm with a low polydispersity index.

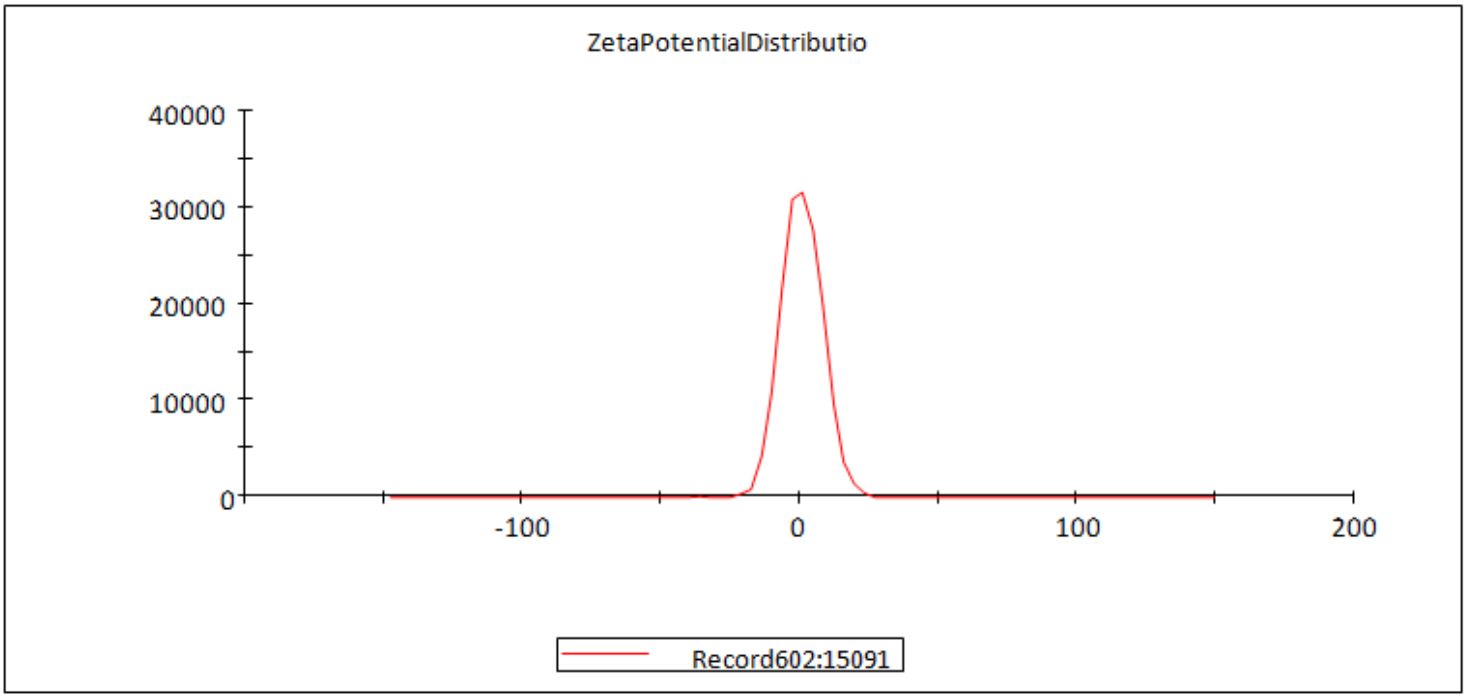

Figure 7

ZETA potential of GSNiNPs: The Zeta potential analysis of GSNiNPs demonstrated that it has positive charges of 0.979 mV.

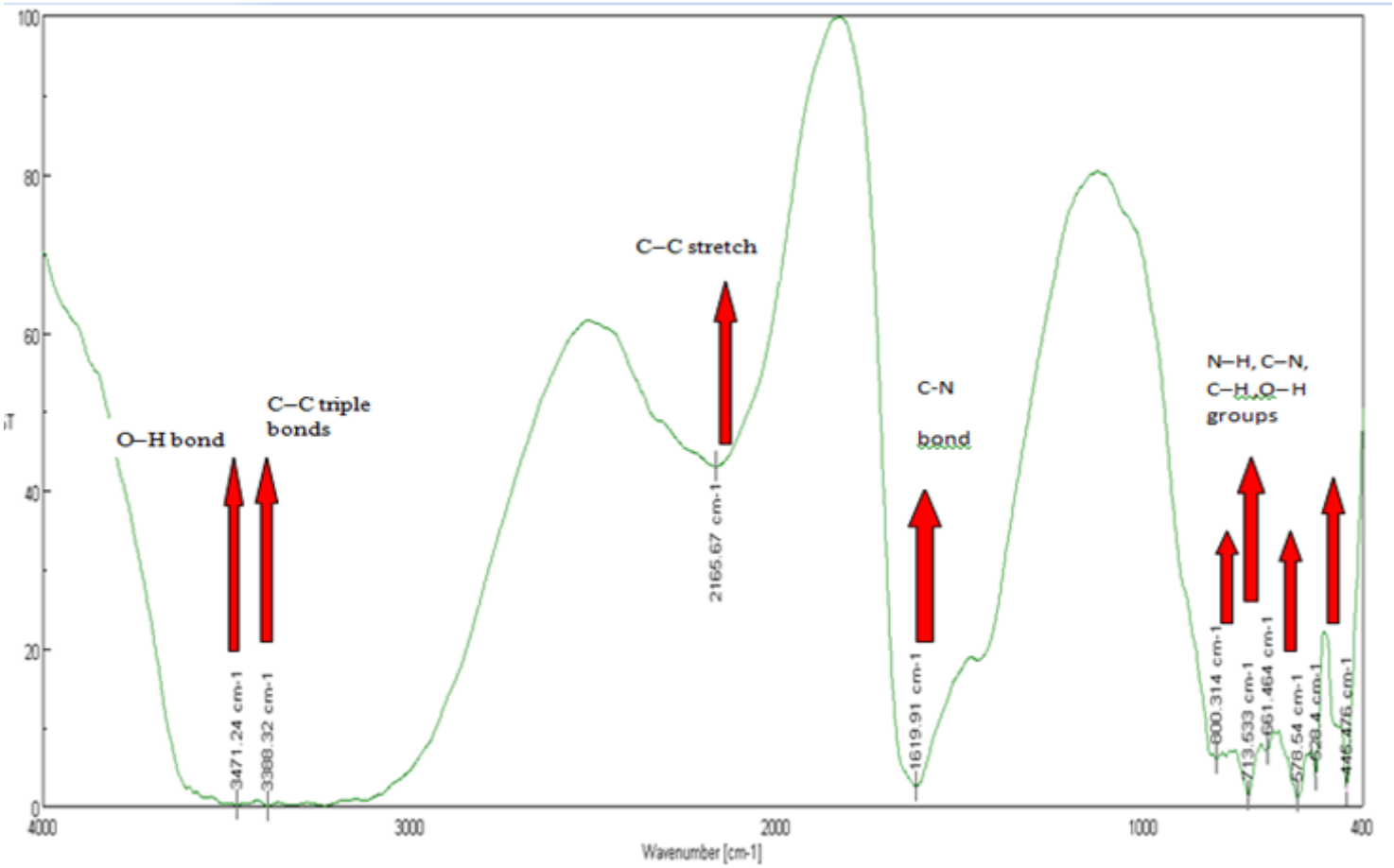

Figure 8

FTIR results of GSNiNPs: FTIR analysis results revealed the functional groups present in GSNiNPsand also showed different stretches of bond present in the compound.

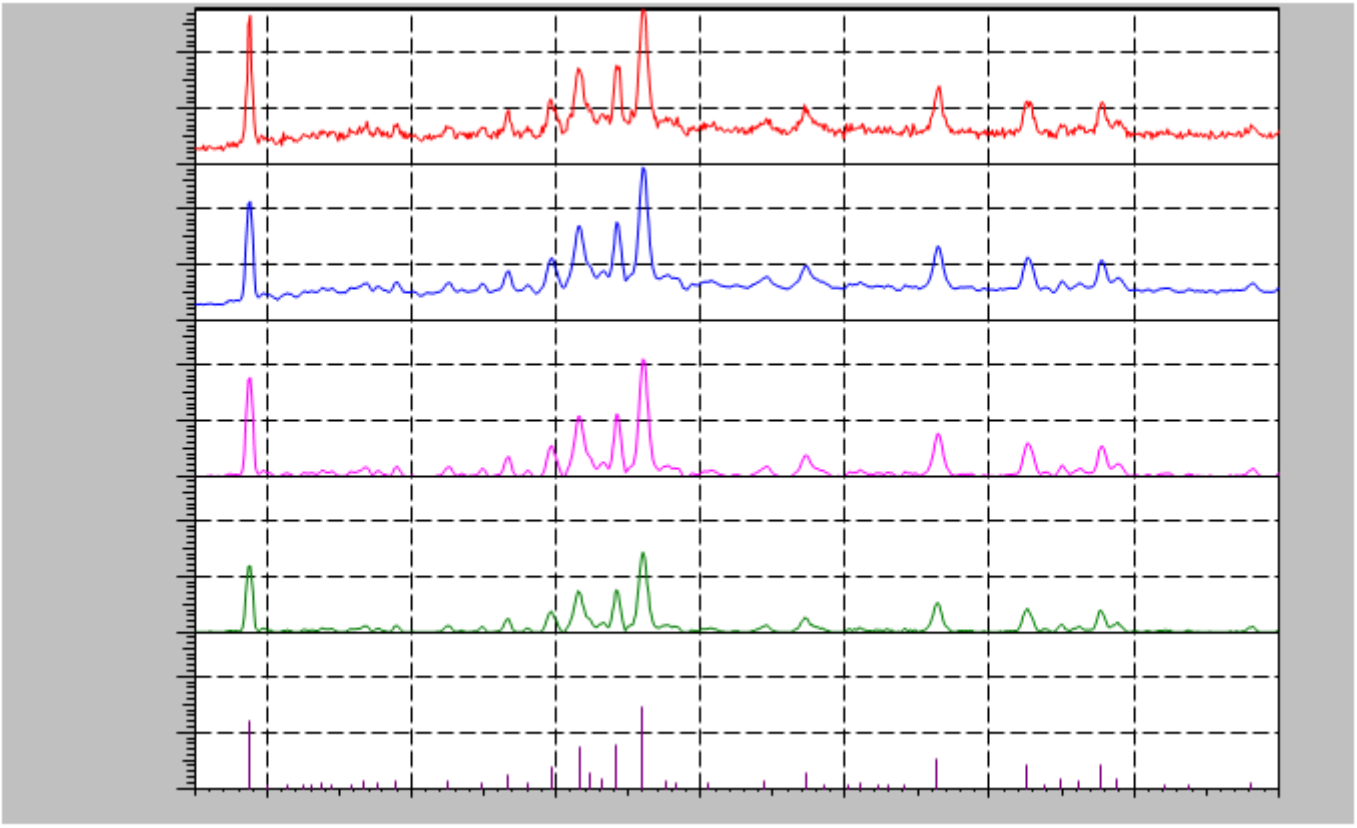

Figure 9

XRD result of GSNiNPs: The XRD pattern of the biosynthesized GSNiNPs shows three diffraction peaks at 2Φ= 20.4500, 16.0795 and 32.9591.

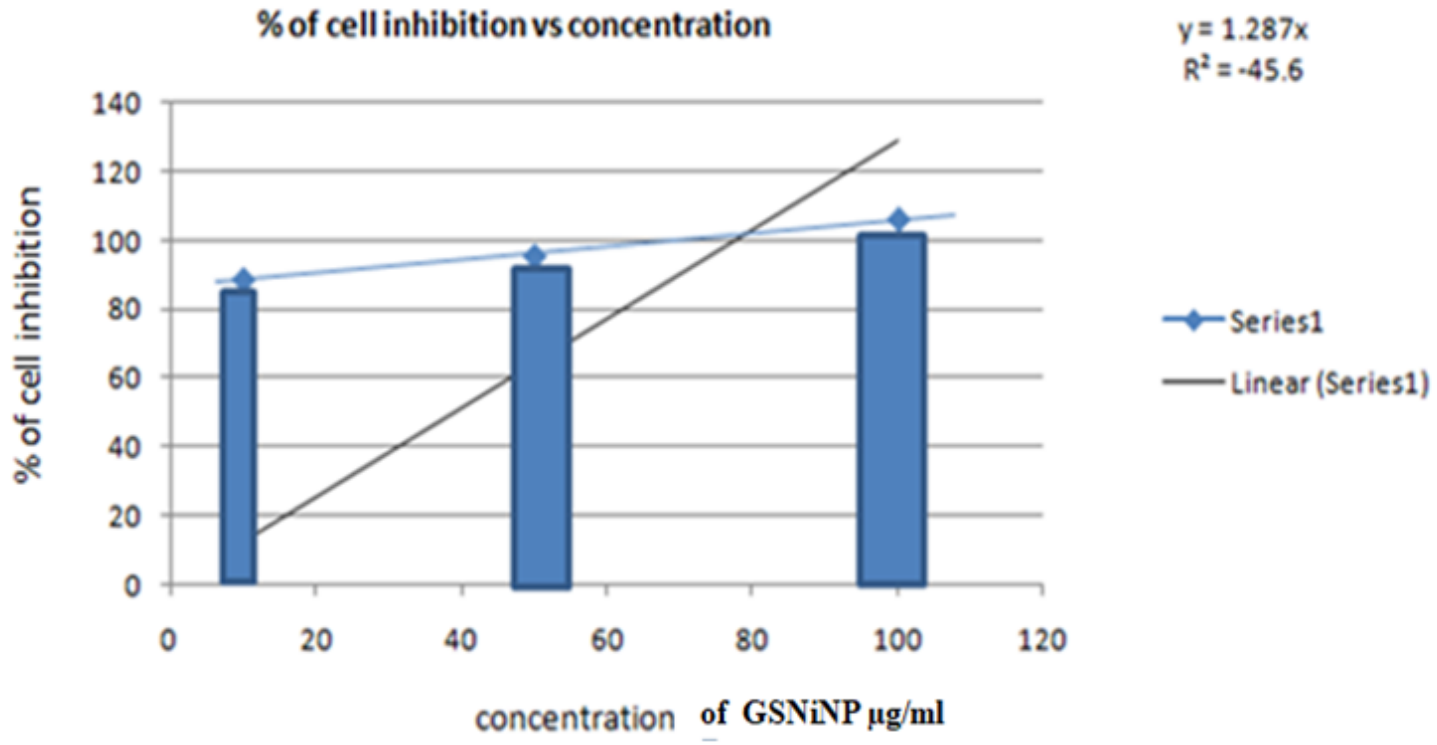

Figure 10

MTT assay of GSNiNPs: The result revealed that the IC_{50} value of the GSNiNPs was found to be 38.85µg/ml.

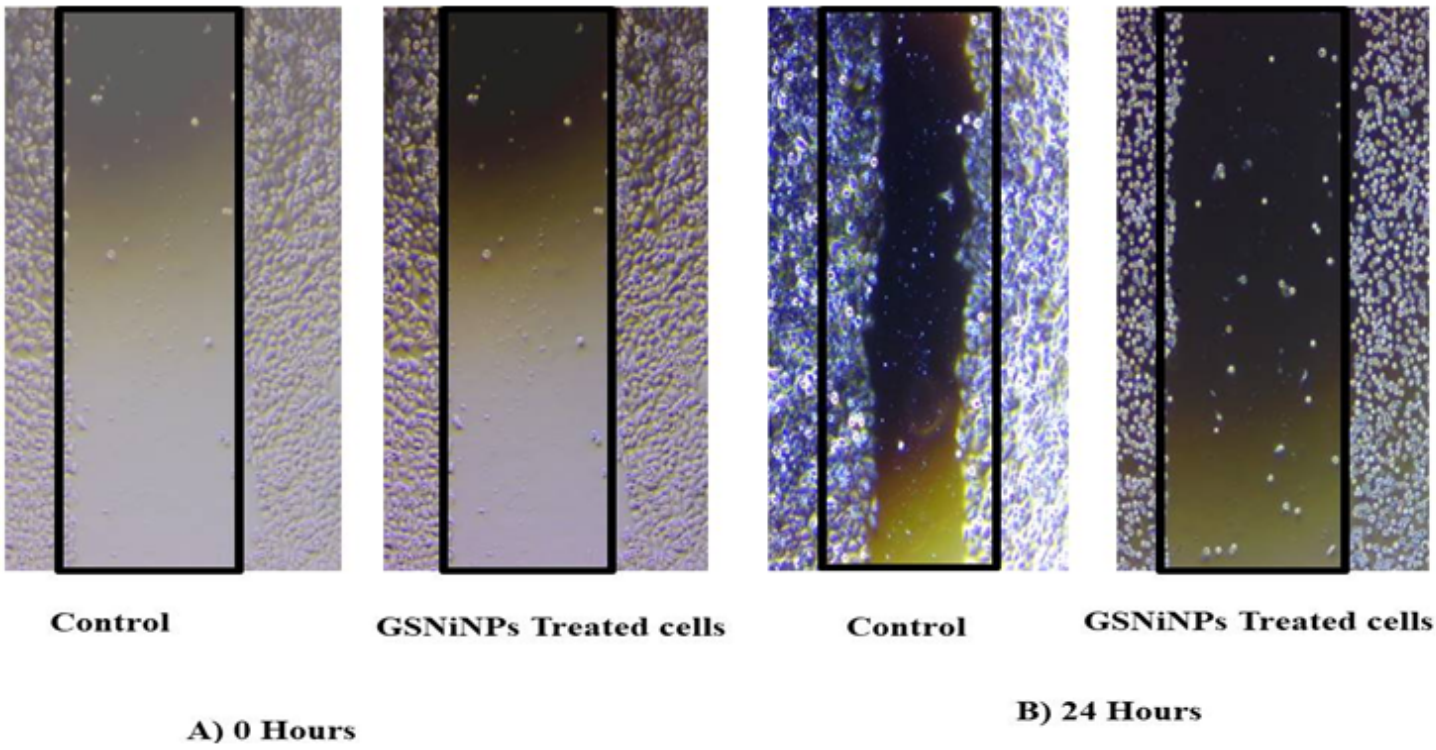

Figure 11

Effect of GSNiNPs on migration capability of HeLa cells: The results revealed that GSNiNPs have the capacity to inhibit the migration and invasion of the cells. From the results it revealed that wound scratch in untreated cells (control) was started to close after 24 hours of incubation, whereas GSNiNPs co treated group suppressed the effect of migration of HeLa cell lines.

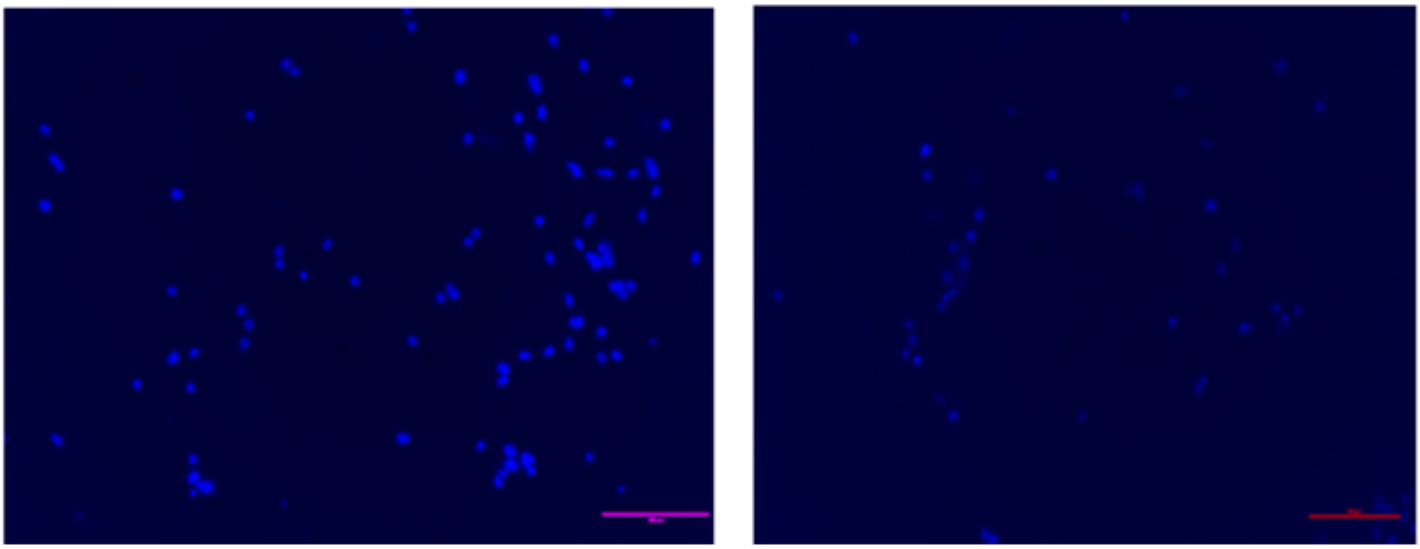

Figure 12

Nuclear morphological DAPI staining images of HeLa cells:It was noted that the number of cells showed the signs of apoptosis (the cells that have brightly fluorescence and fragmented nucleus) in the extract-treated group when compared to the control group.

Figure 13

Detecion of apoptosis by acridine orange and ethidium bromide double staining: Detection of apoptosis by acridine orange and ethidium bromide double staining. a) The control cells emit green fluorescence which reveals that the cells did not undergo apoptosis. b) The cells treated with the desired concentration of**GSNiNPs**undergo early and late apoptosisand emit yellow and reddish-orange fluorescence (indicated by yellow, blue and red arrows).

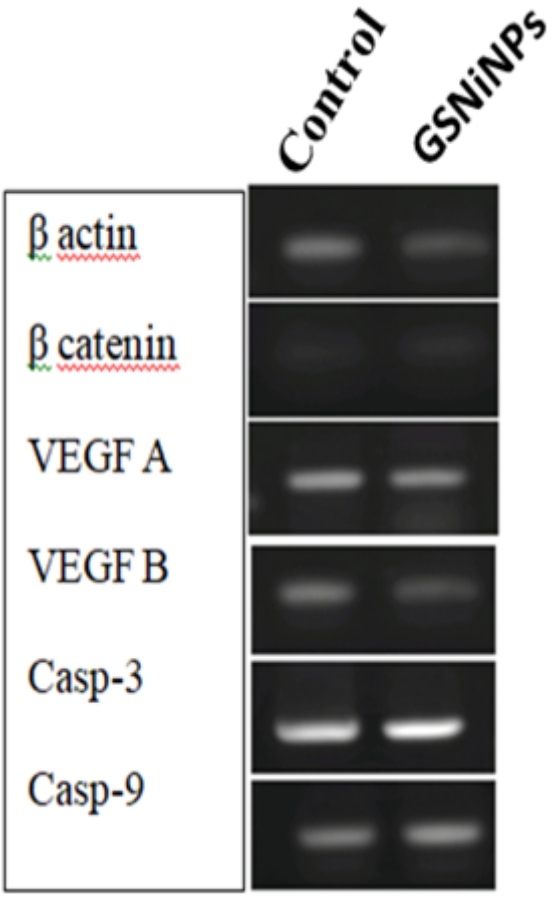

Figure 14

Effect of GSNiNPs on expression of apoptotic related gene: The expression of VEGF A and B were relatively higher in HeLa cells. GSNiNPs treated cells significantly suppresses the expression of VEGF A and B and enhances caspase 3 and 9 at mRNA levels in a dose-dependent manner in HeLa cell lines.